All Solid-State High-Efficiency Tunable UV Source for Airborne or Satellite-Based Ozone DIAL Systems

Darrell J. Armstrong and Arlee V. Smith

***Abstract*—We designed, built, and tested two laboratory prototype nanosecond UV sources for airborne or satellite-based ozone differential absorption lidar (DIAL) remote-sensing systems. Our prototypes use a 532-nm second-harmonic pulse from a *Q*-switched injection-seeded Nd:YAG laser to pump an optical parametric oscillator (OPO) that generates a tunable signal wavelength near 803 nm. The OPO signal is mixed with additional 532 nm light either inside the OPO cavity, or in a subsequent sum-frequency generation (SFG) stage, to generate 10-ns pulses at 320-nm. Our system designs result from an integrated, iterative approach where operating parameters including the pump-beam's spatial profile, the second harmonic generation efficiency, the OPO's cavity geometry, output coupling, crystal lengths, and the length of the SFG crystals, are all determined from numerical modeling. By using this approach, we obtained 320 nm pulse energies approaching 200 mJ with overall optical conversion efficiency—from 1064 to 320 nm—exceeding 20%. To optimize efficiency, we incorporate three important design characteristics: a pump beam having a high-quality flat-topped spatial profile, an image-rotating nonplanar ring-cavity OPO capable of generating high-quality large-diameter flat-topped beams, and pulse injection seeding of the OPO to achieve near-zero cavity buildup time to enhance the efficiency of sum-frequency mining. We believe additional optimization of our designs may eventually yield UV pulse energies approaching 300 mJ with optical conversion efficiencies comparable to those of our current systems.**

***Index Terms*—Frequency conversion, nonlinear optics, optical parametric oscillator (OPO), remote sensing, UV generation.**

I. Introduction

TUNABLE sources of nanosecond UV light with energies exceeding 100 mJ are an enabling technology for a wide range of active remote-sensing applications, including measurements of stratospheric ozone concentration, detection of chemical and biological warfare agents, and standoff measurements of material signatures. These missions often require interrogating large geographical areas, so active sensing systems achieve greatest utility when deployed on unmanned aerial vehicles (UAVs) or on satellite platforms. However, for tunable sources with $\geq$100 mJ UV energies to be practical on mobile platforms, they must have high wall-plug electrical efficiency and fit within small payload volumes. Near-IR diode-pumped solid-state (DPSS) lasers such as Nd:YLF or Yb:SFAP might achieve wall-plug efficiency $\geq$10% in a small volume. However, converting near-IR laser light to the UV requires several successive frequency conversion steps, including second harmonic (2ω) or third harmonic (3ω) generation, additional nonlinear conversion using an optical parametric oscillator (OPO) or optical parametric amplifier (OPA), and a final frequency doubling or sum-frequency generation (SFG) stage. In principle, nonlinear frequency conversion can attain high efficiency; however, in practice, the overall optical efficiency—from the pump-laser wavelength to tunable UV—rarely exceeds 10% so the net wall-plug efficiency of high-energy UV generators is typically $<$1%.

Low efficiency is not a fundamental characteristic of nonlinear frequency conversion, but its efficiency is diminished by light sources with poor beam quality, and further diminished by pump lasers and OPOs that oscillate on multiple longitudinal modes. For example, SFG usually involves mixing beams from two different light sources in a $\chi^{(2)}$ nonlinear crystal, and SFG efficiency is highly sensitive to the coherence properties of the beams. For high efficiency, the two beams must share near-identical spatial properties—preferably high-quality flat-topped profiles of equal diameter—and have temporally transform-limited pulses of near-identical length for optimum spectral and temporal overlap. Because it is difficult for two different sources to simultaneously meet these requirements, SFG efficiency is often $<$10%. If one beam originates from a nanosecond OPO (ns OPO), its beam quality will likely be poor, especially for energies $\gtrsim$20 mJ, so expecting SFG efficiency to reach even 10% may be unrealistic. Placing an SFG crystal inside an OPO cavity and using an injection-seeded pump laser can improve UV efficiency [1], but conventional cavity designs and free-running oscillation in the OPO appear to limit fundamental-to-UV optical efficiency to $\leq$5%.

Given the importance of good beam quality for efficient SFG, and that ns OPOs are integral to most UV-generation systems, we devoted substantial effort to developing an OPO cavity that generates high-quality beams. Beam quality for conventional ns OPO cavities strongly depends on the ratio of pump-beam diameter D to the OPO cavity length L through the cavity Fresnel number $\mathcal{F} = D^2/\lambda L$, where λ is the resonant wavelength. Because $\mathcal{F}$ is a measure of the number of Fresnel zones and indicates the strength of diffractive coupling, low $\mathcal{F}$ results in good beam quality, while large $\mathcal{F}$ tends to result in very poor beam quality. Consequently, when $\mathcal{F}$ approaches one, OPO beam quality becomes quite good. However, an OPO that generates pulses containing tens to hundreds of millijoules requires large pump-beam diameters to maintain fluences well below the damage thresholds of crystals and dielectric coatings. In this case, $\mathcal{F} \geq 100$ is not uncommon, and beam quality suffers inevitably. To accommodate large $\mathcal{F}$, we developed an image-rotating

Manuscript received October 31, 2006; revised March 26, 2007. This work was supported in part by Sandia, a multiprogram laboratory operated by Sandia Corporation, a Lockheed Martin Company for the U.S. Department of Energy's National Nuclear Security Administration, under Contract DE-AC04-94AL85000 and in part by the NASA Langley Research Center, Hampton, VA.

The authors are with Sandia National Laboratories, Albuquerque, NM 87185-1423 USA (e-mail: darmstr@sandia.gov; arlsmit@sandia.gov).

Digital Object Identifier 10.1109/JSTQE.2007.896600

nonplanar ring-cavity OPO, where image rotation works in conjunction with angle-critical birefringent phase matching in bulk crystals to greatly improve beam quality [2]–[4].

The spectral and temporal properties of the frequency-summed beams are also important for SFG efficiency, so we devoted our efforts to improving them as well. For a pump laser such as Q-switched Nd:YAG, operation near the transform limit requires no more than injection seeding using a low-power continuous-wave (CW) laser. However, for ns OPOs, obtaining equivalent performance is more difficult because two conditions must be met: single-frequency oscillation and effectively instant startup the moment the pump pulse arrives. When OPOs start up from quantum fluctuations in the signal and idler fields, cavity buildup time can be a substantial fraction of the pump pulse length, especially near the oscillation threshold. Injection seeding the OPO using a low-power CW laser achieves single-frequency oscillation, but reduces buildup time by approximately 1 ns, which is insufficient for achieving complete temporal overlap with the undepleted pump pulse, as required for high-efficiency SFG. A multi-kilowatts CW seed source might reduce OPO buildup time to near zero but is obviously impractical. The only way to achieve early turn-on, or equivalently, an OPO with an oscillation threshold of near zero pump energy, is through pulsed injection seeding. The intracavity optical power obtained by coupling a seed pulse with $\lesssim$1 mJ into the OPO cavity easily exceeds the power circulating in the cavity at threshold, so that oscillation occurs the moment the pump arrives. Such pulsed injection seeding increases complexity, but we found it improved SFG efficiency by 10%–30%, so we developed pulse seeding techniques to compliment the improvements in beam quality from our image-rotating OPO [5].

Combining a 10% wall-plug efficient pump laser with a UV-generating system having 20% optical-to-optical efficiency would result in 2% wall-plug efficiency. However, meager that may sound, 2% overall electrical-to-optical efficiency might represent an improvement by a factor of 2 over UV generators using traditional OPO cavity designs and traditional injection seeding techniques. For deployment on UAVs or satellites, that translates to a significant halving of the required electrical power for the equivalent optical output.

In this paper, we will illustrate how intracavity image rotation improves beam quality in ns OPOs, and describe how pulsed injection seeding reduces buildup time to enhance SFG efficiency, and results in pump depletion in the OPO as high as 90%. We will also describe two different methods of implementing SFG to generate 320 nm light: one being "extracavity" with the SFG crystal external to the OPO and the other "intracavity" with the SFG crystal inside the OPO cavity. We will also show results for a complete UV-generation system with overall optical efficiency—from 1064 to 320 nm—exceeding 20% for 320 nm pulse energies approaching 200 mJ. Finally, we will describe current and future work intended to improve on these results.

II. Nonplanar Ring-Cavity Image-Rotating OPO

To illustrate how intracavity image rotation improves beam quality in ns OPOs, we compare output beams from two different singly resonant cavities: a conventional three-mirror ring and a four-mirror nonplanar ring that induces 90° of intracavity image rotation. Both OPOs were pumped by the same injection-seeded Nd:YAG laser with a beam diameter of $\sim$6 mm. The pump's spatial fluence profile was globally flat but locally modulated by circular diffraction rings arising from overfilled amplifier rods. The pump wavelength was 532 nm with full-width at half-maximum (FWHM) pulse duration of 10 ns, and both OPOs were injection seeded to oscillate single-frequency at $\lambda_{\rm signal} = 803$ nm, with $\lambda_{\rm idler} = 1576$ nm. The same 15-mm-long antireflection-coated potassium titanyl phosphate (KTP) crystal having a $10\,{\rm mm} \times 10$ mm aperture was used in both OPOs. The crystal was cut for propagation in the xz-plane at 58.4° for $532({\rm o}) \rightarrow 1576({\rm o}) + 803({\rm e})$, where "o" and "e," respectively, denote ordinary and extraordinary waves, and the arrow denotes the direction of energy flow. The walkoff angle for the 803 nm e-wave was 47.4 mrad.

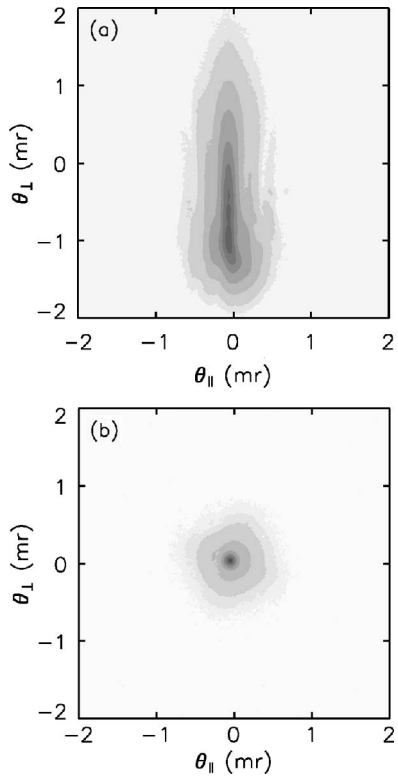

Fig. 1. (a) Contour plot of the far-field signal spatial fluence profile for a three-mirror ring-cavity OPO with Fresnel number $\mathcal{F} \approx 300$. (b) Corresponding measurement for a four-mirror nonplanar ring cavity OPO with 90° of intracavity image rotation and $\mathcal{F} \approx 400$. $\theta_\parallel$ and $\theta_\perp$ denote, respectively, the far-field angles parallel and perpendicular to the direction of birefringent walkoff. Both OPOs were pumped by an $\sim$6 mm diameter beam. See text for additional details.

The lengths of the cavities differed by approximately 40 mm, with $L \approx 150\,{\rm mm}$ for the three-mirror ring, and $L = 109\,{\rm mm}$ for the image rotator, resulting in $\mathcal{F} \approx 300$ and $\approx$400, respectively. Although their lengths differed, comparing beam properties for the two cavities to illustrate a point is valid because all other experimental parameters were similar.

Fig. 1(a) shows a contour plot of the far-field signal spatial fluence profile for the three-mirror ring-cavity OPO plotted against far-field angles $\theta_\parallel$ and $\theta_\perp$, and Fig. 1(b) shows the

equivalent measurement for the image-rotating cavity. Here, $\parallel$ and $\perp$ refer to the directions parallel and perpendicular to birefringent walkoff. The difference in beam quality in Fig. 1(a) and (b) in the perpendicular direction is large, but the difference is much smaller in the parallel direction, suggesting walkoff somehow "cleans up" the beam.

Physically, walkoff smoothes the phase, or more rigorously, increases phase front correlation, across one transverse dimension of the beam. This process occurs over a distance equal to the Poynting vector walkoff displacement each time the OPO's resonated wave passes through the nonlinear crystal. Although the better beam quality observed in the angle-critical direction can be attributed to the small acceptance angle for a particular mixing process, visualizing beam cleanup in terms of phase correlations induced by birefringent walkoff may improve physical insight.

Understanding that birefringent walkoff is the mechanism that improves beam quality suggests transferring this mechanism to the orthogonal transverse dimension of the beam—and that can be done using image rotation. With image rotation, walkoff increases phase correlation within a rectangular region that rotates by 90° for each pass through the crystal, and consequently, it continuously increases in size. For a pump pulse that is sufficiently long relative to the cavity round-trip time, this correlation can extend over the OPO's entire beam profile. The result is a beam with a high degree of phase front correlation in both transverse dimensions that approaches the diffraction limit under ideal mixing conditions. The far-field fluence profile in Fig. 1(b) is not diffraction limited; however, approximately 60% of the focused energy falls within this limit, which is a good result for an ns OPO with $\mathcal{F} \approx 400$.

In all OPO cavities, beam quality is best when undesirable pump-beam characteristic have least influence on the resonated wave. For our two example OPOs, we chose mixing where the pump and idler shared o-polarization with $532(\mathrm{o}) \rightarrow 1576(\mathrm{o}) + 803(\mathrm{e})$, and the signal—which walks off from the idler and pump—was a mode of the cavity. Switching polarizations so that $532(\mathrm{e}) \rightarrow 1576(\mathrm{e}) + 803(\mathrm{o})$ would also work well, but using $532(\mathrm{e}) \rightarrow 1576(\mathrm{o}) + 803(\mathrm{e})$, where the pump and signal copropagate, would make the resonated signal susceptible to the beam quality of the pump. Image rotation remains effective in this case, as long as there is walkoff between the o- and e-waves, but the ability to convert a low-quality pump beam to a high-quality signal is diminished by the influence of the pump. We also note that for the fluence profile in Fig. 1(a), walkoff occurred in the plane of the three-mirror cavity so that beam quality was influenced by image inversion. Had we used a more common two-mirror linear cavity that lacks image inversion and that is more susceptible to the deleterious effects of double, or even triple resonance, the beam quality in Fig. 1(a) would be worse.

The benefits of image rotation can be obtained by using many different cavity designs, but all involve additional complication and cost. Image-rotating cavities require an intracavity $\lambda/2$ retarder to orient polarization of the circulated waves parallel to the eigenpolarizations of the nonlinear crystal, and some also require intracavity prisms [2], [3]. Because low- or zero-order

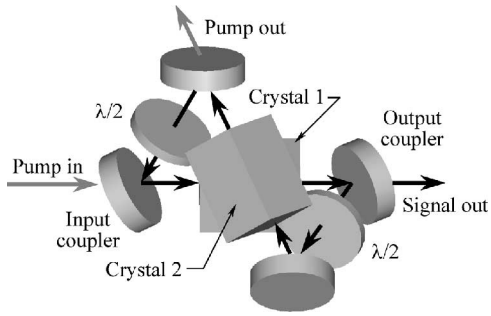

Fig. 2. Geometric configuration of a two-crystal RISTRA OPO cavity. Two long legs contain crystals and two short legs contain $\lambda/2$ plates, with the ratio of their physical lengths being $\sqrt{2}$. The angle of incidence on all cavity mirrors is 32.8°, and the nominal physical length of the cavity is 109 mm. For two crystals, the wave plate in the horizontal leg must have retardation of $\lambda/2$ for the pump and resonated wave. For a one-crystal configuration, crystal 2 is removed and the wave plate in the vertical leg is not required.

$\lambda/2$ plates may not be available for the entire visible to mid-IR operating range of ns OPOs, some image-rotating designs may be poorly suited to applications requiring tunability $\gtrsim$10 nm. However, image rotators are very well suited to applications requiring large beam diameters at a single wavelength, such as generating high-energy UV.

While developing our image-rotating cavity we tested various geometric configurations and found some of them awkward to work with in the laboratory. We settled on a nonplanar four-mirror ring-cavity configuration known as the rotated image singly-resonant twisted rectangle (RISTRA) whose design is described in detail in [4]. As its name implies, the RISTRA begins as a planar rectangle that is twisted, so the resonated wave experiences 90° of image rotation for each trip around the cavity. The cavity configuration for a two-crystal RISTRA is shown in Fig. 2. For one-crystal oscillation, the crystal in the tilted path and the second $\lambda/2$ plate are removed, and the pump exits through the output coupler. Owing to the nonplanar geometry, longitudinal modes of the RISTRA will translate laterally under the effect of small tilts of its cavity mirrors, but they still close to form a mode, so the RISTRA can be constructed as a quasi-monolithic cylinder having no cavity mirror adjustments, as shown in Fig. 3. Cavity mirrors are held against three-point machined faces on the cylinder by corresponding three-point spring-loaded retainers making the design simple and mechanically robust. The RISTRA also possesses a high degree of spatial symmetry, so the propagation direction of the resonated wave can be reversed to accommodate the polarization orientation of various crystal cuts. For example, the propagation direction shown in Fig. 2 is best for an o-polarized pump incident on the input coupler as a p-wave, and for circulating an e-polarized resonated wave. Reversing the propagation direction and the locations of the cavity mirrors accommodates a crystal cut for the orthogonal polarizations.

III. Flat-Topped Beam Profiles and Pulse-Injection-Seeded OPOs: Requirements for High-Efficiency SFG

To generate approximately 200 mJ of 320-nm light with high efficiency, we selected operating parameters for the final SFG

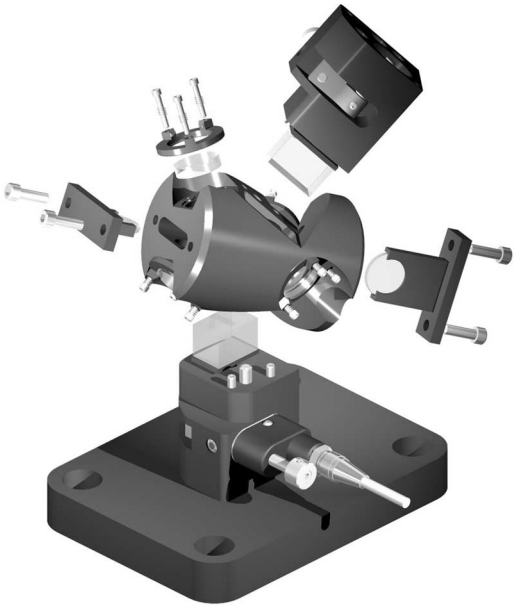

Fig. 3. Exploded solid rendering of two-crystal RISTRA cavity assembly showing cylindrical body, spring-loaded three-point mirror retainers and mirror substrates, wave plate holders, and crystal rotation assemblies. Owing to its nonplanar geometry, the RISTRA requires no cavity mirror adjustments. See text for additional details.

stage and worked back through the system, defining OPO and pump-beam requirements accordingly. These requirements include flat-topped beam profiles with diameters of 6–8 mm for the 532 nm pump beam and for the OPO's 803 nm beam, and they also require the pulse for each to be of equal duration and temporally transform limited. Our injection-seeded pump laser met these requirements following modifications to improve its beam quality [6]; however, designing an OPO that meets these requirements involves a considerable effort. As described in Section II, image-rotating OPO cavities produce high-quality beams, and as discussed in Section I, pulse injection seeding an OPO can reduce its cavity buildup time to near zero. However, cavity geometry and injection seeding do not necessarily force an OPO to generate a flat-topped beam. From modeling and previous measurements, we found that when an OPO's pump beam is spatially flat, the spatial profile of the pulsed seed beam strongly influences the spatial profile of the OPO's resonated wave. Consequently, we prepared a flat-topped pulsed seed beam with its diameter matching that of the pump. The injection-seeded OPO then generated a flat-top signal beam in the near field, which resulted in pump depletion in the OPO as high as 90% [5].

Beams having flat-topped spatial profiles increase the efficiency of three-wave mixing in $\chi^{(2)}$ nonlinear crystals, and their importance to our UV system cannot be overstated. The reason is simply that conversion efficiency is greater using flat-topped beams because the irradiance-dependent strength of nonlinear mixing is uniform across the beam profiles. This is true for SFG, where combining flat spatial profiles with temporally transform-limited pulses enhances "photon balance," so that the two frequency-summed pulses are depleted equally. It is also true for ns OPOs, where flat spatial profiles mitigate the efficiency-robbing effects of parametric back-conversion, where the signal and idler can mix to generate new pump light. To appreciate the importance of flat-top beams, consider an ns OPO pumped well above its oscillation threshold by a Gaussian beam, where the irradiance is high on axis and low in the wings. Shortly after oscillation begins, the pump will deplete essentially 100% on axis, and immediately thereafter back-conversion generates new pump light that is 180° out of phase with the original pump. The complex temporal dynamics and π-phase shifted pump-light occurring on axis, but not in the wings of the Gaussian, reduce beam quality and conversion efficiency. In addition, walkoff of e-waves introduces spatial asymmetry by translating irradiance-dependent back-conversion effects across the beam profile. These effects can be numerically modeled [7], [8],[1] and were experimentally observed in time-resolved measurements of OPO pulse temporal evolution [9]. While elimination of back-conversion is desirable, it cannot be eliminated altogether. However, its onset at a specific pump energy can be selected to some extent, thereby preserving OPO beam quality for a desired output energy. We try to select this operating point for our pulse-injection-seeded OPOs by appropriately choosing crystal lengths and output coupling.

There are several ways to pulse injection seed ns OPOs, including the use of a single-frequency tunable pulsed laser or OPO as an independent auxiliary source, or alternatively, having the OPO generate its own seed pulse, which we call "self-seeding." The energy required for the seed pulse is $\lesssim$1 mJ, but its duration must result in a spectral Fourier transform that overlaps only one longitudinal mode of the OPO cavity. For self-seeding, a low-energy pump pulse arrives in advance of the main high-energy pump, generating a seed pulse that is subsequently reinjected into the OPO. Our implementation of self-seeding uses "backward pumping," with a backward-propagating CW seed beam locked to a cavity resonance to generate the single-frequency seed pulse. It also used two pump lasers to simplify control of pump-pulse arrival times, as shown in Fig. 4. Self-seeding is practical because it eliminates the need to frequency-stabilize one pulsed oscillator relative to another, and because the seed-pulse spectrum automatically matches the OPO's cavity resonances. Because the seed resonantly couples into the OPO cavity, and is briefly stored by the cavity, it must arrive approximately one pump-pulse length in advance. We found the control of arrival time within $\pm$1 ns sufficient for stable shot-to-shot OPO signal output when using 8–10 ns pump pulses.

As described earlier, the key to achieving high-efficiency SFG in our system is to force the OPO to generate a flat-topped signal beam for mixing with the undepleted flat-topped pump. Fig. 4 shows an optical network that spatially modifies the seed pulse

[1]Numerical models for nonlinear mixing in crystals for time scales ranging from femtoseconds to CW are available in the Sandia Non-Linear Optics (SNLO) software package package, written and distributed by Arlee V. Smith at Sandia National Laboratories. SNLO contains 17 different software tools that can be used for design and testing of OPAs, OPOs, and to calculate nonlinear crystal mixing parameters. SNLO can be downloaded free of charge from http://www.sandia.gov/imrl/XWEB1118/xxtal.htm. Special codes for various versions of the image-rotating RISTRA OPO used in our high-energy UV systems, including those for intracavity SFG, are available on request.

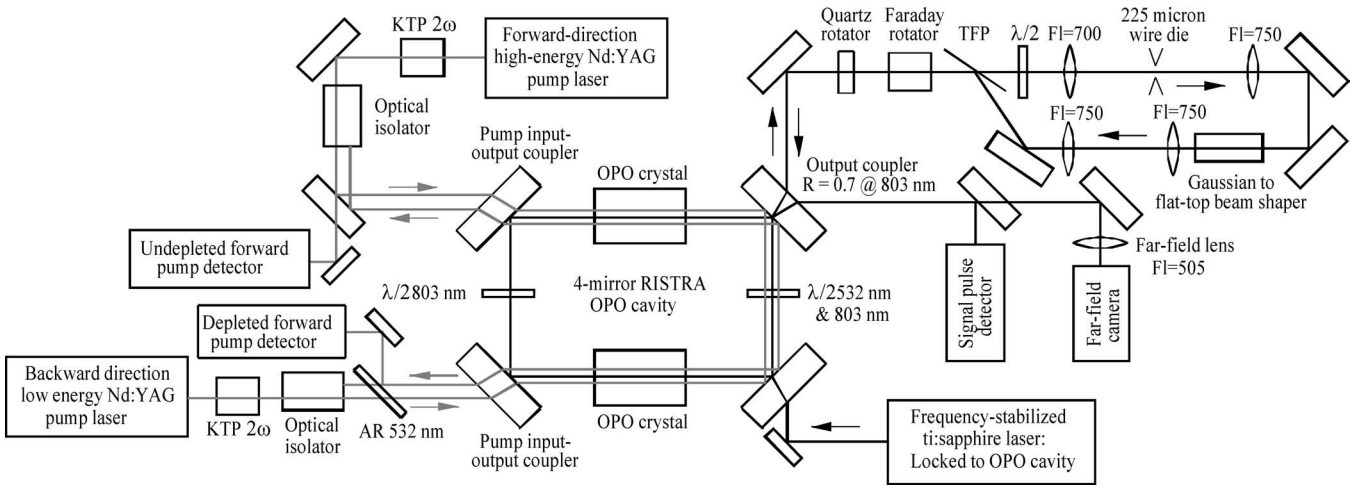

Fig. 4. Block diagram of backward-pumped self-injection-seeded RISTRA OPO. The nonplanar RISTRA cavity is projected onto the plane of the page for clarity. In the experiment, the 109-mm-long cavity contains two 10 mm × 10 mm × 15 mm KTP crystals cut at $\theta = 58°$, $\phi = 0°$ for $532(\mathrm{o}) \rightarrow 803(\mathrm{e}) + 1576.4(\mathrm{o})$. The two intracavity $\lambda/2$ retardation plates maintain pump and signal polarizations parallel to the crystal's eigenpolarizations. Approximately 5 mW of 803 nm light from a frequency-stabilized CW Ti:Sapphire laser (Coherent 899) is dither-locked to a cavity fringe using phase-sensitive detection, so the laser providing a small-diameter low-energy backward-direction pump beam (Q-switched injection-seeded Nd:YAG, Continuum NY82-10) generates a 2-mm $1/e^2$ diameter single-frequency 5 mJ seed pulse. The seed pulse returns to the cavity via the optical path containing a spatial filter, Gaussian to flat-top refractive beam shaper (Newport GBS-AR16), and imaging telescope, with maximum energy measured at the thin film polarizer (TFP) >1.5 mJ. The 6 mm diameter spatially flat pulsed seed resonates in the cavity and is amplified by the time-delayed forward pump laser (Q-switched injection-seeded Nd:YAG, Continuum PL-9010). The PL-9010 was modified so that it produces a high-quality flat-top profile with diameter closely matching that of the pulsed seed beam [6]. Relative arrival times of the pulses are controlled to ∼1 ns by externally triggering the pump lasers using clock-synched digital delay generators (SRS DG535). Signal and forward pump detectors are Hamamatsu R1328U vacuum photodiodes with bandwidths of ∼5 GHz. Focal lengths are in millimeters.

for this purpose. It consists of a spatial filter followed by a Gaussian to flat-top refractive beam shaper (NRC model GBS-AR18), along with imaging optics and an optical diode. We found that seed pulse energies as low as 50 μJ reduced buildup time to about 1/10th of the pump pulse duration and forced the OPO to produce a flat-top signal profile in the near field. For seed energies near 1 mJ, there was no change in the signal spatial profile, but buildup time was near zero, resulting in a signal pulse temporal profile indistinguishable from the temporal profile of the undepleted pump. Fig. 5 compares temporal profiles for unseeded oscillation, pulse-injection-seeded oscillation using flat-topped pump and seed beams, and pulse-injection-seeded oscillation using a flat-topped pump and Gaussian seed profile. These measurements demonstrate the need for flat-topped beam profiles.

IV. Two Configurations for Generating UV: Extra- and Intracavity SFG

We generated 320-nm light using two experimental configurations; in the conventional approach, extracavity SFG mixes two beams in a crystal outside the OPO cavity, and for intracavity SFG, the unconventional approach, the sum-frequency mixing crystal is inside the OPO. Various intracavity upconversion methods have been reported experimentally using various pump lasers, including ruby-pumped 2ω [10], mode-locked Nd:YAG pumped SFG [11], [12], mode-locked Ti:sapphire pumped SFG [13], and theoretically using plane-wave approximations for separate OPO and SFG crystals [14], and also for one crystal that phase matches for oscillation and SFG [15]. In our experiments, the OPOs in either configuration oscillate an 803 nm signal using type II KTP cut for propagation in the xz-plane at $58.4°$ with $532(\mathrm{o}) \rightarrow 1576(\mathrm{o}) + 803(\mathrm{e})$, and both configurations were pumped and pulse-injection-seeded using flat-topped beams, as described previously. We found extracavity SFG produced higher UV energy but requires more optical components, careful alignment of beams, and accurate control of pulse arrival times, to optimize mixing efficiency in the external SFG crystal. Intracavity SFG requires fewer optical components, obtains higher efficiency from the cavity-enhanced signal power, and beam alignment and timing for SFG occur automatically inside the cavity. However, risk of optical damage and absorptive heating effects may limit the use of intracavity SFG to lower UV energies.

For extracavity SFG, the OPO is identical to that shown in Fig. 4 with two 15-mm-long KTP crystals with 10 mm × 10mm apertures. The output coupler has $R = 0.7$ at $\lambda = 803$ nm and $R > 0.98$ at $\lambda = 532$ nm. In addition, the mirror where the 803 nm CW seed beam enters the cavity also has $R > 0.98$ at $\lambda = 532$ nm so that forward and backward pumps pass through both crystals before leaving the cavity through one of two pump-input/output couplers. The extracavity SFG crystal shown in Fig. 6 is type I β-barium borate (BBO) cut at $36.6°$ for $803(\mathrm{o}) + 532(\mathrm{o}) \rightarrow 320(\mathrm{e})$ with length of 8 mm and aperture of 10 mm × 10mm. Although the walkoff angle is large at 79 mrad and the acceptance angles correspondingly small at 0.61 and 0.40 mrad·cm, type I mixing was selected because $d_{\mathrm{eff}} = 1.95$ pm/V compared to 0.92 or 0.36 pm/V, respectively, for either type II SFG cut of BBO.

Using two 15-mm-long crystals in the OPO for extracavity SFG resulted not only in very high efficiency at very low pump fluence [5], but also in earlier-than-desired onset of strong back-conversion. To maintain optimum efficiency, we operated

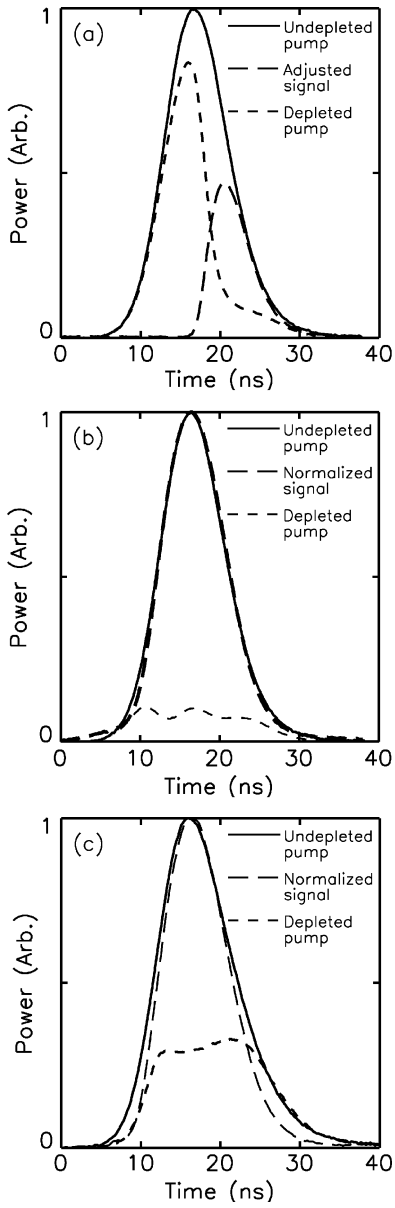

Fig. 5. (a) Measured undepleted pump, depleted pump, and signal temporal profiles for the unseeded two-crystal RISTRA OPO when pumped $\sim 1.5\times$ the threshold for unseeded oscillation. (b) Same three temporal profiles with the same pump fluence but with the OPO self-injection seeded. The pump and self-seed spatial profiles in (a) and (b) are flat-tops. The signal pulse in (a) is adjusted to compare its energy to the normalized signal in (b). (c) Same three signals for higher pump fluence but the pump spatial profile is second-order super-Gaussian (fluence $\propto e^{(-2r^4/a^4)}$ where r is the radius and $a = 1/e^2$ diameter), and the the self-seed profile is lowest order Gaussian. Pump depletion is 85% in (b) but only 52% in (c). In subsequent measurements using a flat-top pump beam and Gaussian pulsed seed, we have recorded self-seeded pump depletion as high as $\sim$65%, but found exceeding this value requires that both beams have flat-top profiles. All temporal profiles in (a)–(c) are averages of 10–20 pulses. See text for additional details.

the OPO with signal output of $\lesssim$25 mJ and added an optional external amplification stage with a gain of 3–5 to boost the signal energy to 100–120 mJ, as shown by the dashed lines in Fig. 6.

For intracavity SFG, the lower KTP crystal shown in Fig. 2 was replaced by a 10 mm $\times$ 10 mm $\times$ 10 mm type II BBO crystal cut at 48.2° for $803(\mathrm{e}) + 532(\mathrm{o}) \rightarrow 320(\mathrm{e})$ with $d_{\mathrm{eff}} = 0.92$ pm/V. This type II cut of BBO is more convenient of the two available cuts because it has larger d_{eff} and maintains 803(e) and 532(o) eigenpolarizations. The lower OPO crystal, rather than the upper, is replaced by the SFG crystal so sum-frequency mixing occurs with an undepleted pump pulse, which is known to enhance the intracavity SFG efficiency [11]. Because oscillation at 803 nm and sum-frequency mixing to generate 320 nm both deplete the 532 nm pump, too much depletion by one mixing process diminishes the overall UV efficiency. The relative lengths of the OPO and intracavity SFG crystals are, therefore, selected by iteratively running the numerical models.

The intracavity experimental configuration differs substantially from Fig. 6 because amplification and external sum-frequency mixing are eliminated. In addition, the output coupler is replaced by one having high transmission for p-polarized $\lambda = 320$ nm light, and also having $R = 0.85$ at 803 nm to enhance intracavity signal fluence and improve SFG efficiency. Although using $R > 0.90$ at 803 nm further improved efficiency in our models, we tested output couplers having $R > 0.90$ and found their damage thresholds to be of the order of 1 J/cm^2, which offers an insufficient margin of safety for practical devices.

For 1064 to 532 nm 2ω generation, we used 10 mm $\times$ 10 mm $\times$ 10 mm xy-cut KTP crystals with conversion efficiency of approximately 71%. The xy-cut of KTP phase matches only for type II mixing with $1064(\mathrm{e}) + 1064(\mathrm{o}) \rightarrow 532(\mathrm{e})$ but has small birefringent walkoff angles of 3.15 and 4.11 mrad, respectively, for the 1064 and 532 nm extraordinary waves. With a high-quality 6–8 mm diameter flat-topped 1064 nm beam, even higher 2ω efficiency is easily obtained by using longer crystals.

Although we have conducted experiments only at 320 nm, UV ozone differential absorption lidar (DIAL) requires two wavelengths, the other being closer to 300 nm. For UV energies >100 mJ, it is impractical to generate two widely separated wavelengths using a single source. Both configurations described here can generate shorter wavelengths by changing crystal cut angles, OPO cavity mirror sets, the intracavity $\lambda/2$ plates, CW injection seed wavelength, and some of the associated optics. For example, to generate $\lambda = 308$ nm requires an OPO signal wavelength of 731.5 nm that can be obtained from xz-cut KTP at $\theta = 51.8^\circ$ with $532(\mathrm{o}) \rightarrow 1950.7(\mathrm{o}) + 731.5(\mathrm{e})$. For extracavity mixing, the BBO crystal is cut at $\theta = 38.6^\circ$ with $731.5(\mathrm{o}) + 532(\mathrm{o}) \rightarrow 308(\mathrm{e})$, and for intracavity mixing, $\theta = 52.4^\circ$ with $731.5(\mathrm{e}) + 532(\mathrm{o}) \rightarrow 308(\mathrm{e})$. We have not tested either SFG configuration at 308 nm.

V. Results and Discussion

For the extracavity SFG configuration shown in Fig. 6, we obtained >190 mJ of 320-nm light at a 10 Hz repetition rate with optical conversion efficiency from 1064 to 320 nm of 21%. For intracavity SFG, the maximum 320 nm energy was $\sim$160 mJ with optical conversion efficiency of 24%. Both injection-seeded pump lasers have shot-to-shot energy fluctuations $\leq$1%, and the pulse-injection-seeded OPOs have shot-to-shot signal-energy fluctuations <1%, so that UV energy fluctuations were of the order of 1%. Nonetheless, the UV energy values are averages because they were measured with a Scientech Model

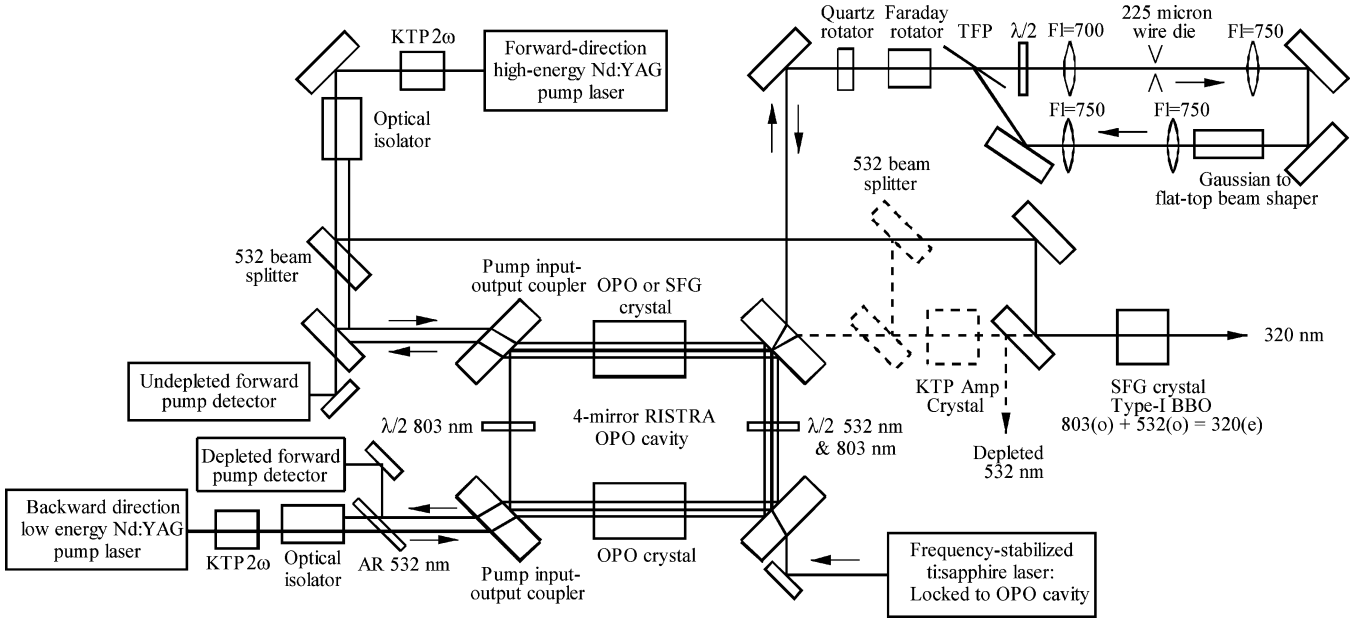

Fig. 6. Simple block diagram of the experiment for extracavity SFG. The OPO, pump lasers, and self-injection seeding apparatus are the same as described in Fig. 4. The 532 beam splitter and additional pump-beam path are required for mixing in the external SFG crystal. The additional dashed lines show an amplification crystal and associated optics required to increase signal energy. Amplification was required because the OPO used for extracavity SFG was originally designed to deplete the pump at very low fluence, as described in [5]. We could not obtain the necessary signal energy without undesirable strong back-conversion in the OPO. See text for additional details.

380101 volume-absorbing detector with settling time of several seconds. For both configurations, our reported conversion efficiencies are calculated by including the 2ω efficiency of approximately 71%; however, we do not carefully account for the energy used for backward pumping. At present, it uses $\gtrsim$20 mJ of 532 nm light, with the 1064 nm fundamental obtained by spatially filtering the low-quality beam from the oscillator of a flashlamp-pumped Nd:YAG laser (Continuum NY82-10). The approximately Gaussian profile of the 1064 nm beam results in low 2ω efficiency, followed by low conversion efficiency in the OPO. If we include the energy used for backward pumping, the total optical conversion efficiency drops by about 1% for each configuration. A laser designed specifically for this purpose would improve the overall conversion efficiency.

The 1064–320-nm conversion efficiency reported here is influenced by three factors: 2ω efficiency, OPO efficiency, and the SFG efficiency. For extracavity mixing, SFG efficiency can be accurately determined by measuring the depletion of the frequency-summed 803 and 532 nm pulses. Our goal was equal depletion of the summed pulses to obtain photon balance and SFG efficiency approaching 60%. As shown by the depleted and undepleted 803 nm pulses in Fig. 7(a) and by the corresponding 532 nm pulses in Fig. 7(b), the measured depletion was not well balanced. When the 532 nm beam splitter for the optional amplification stage in Fig. 6 had $R = 50\%$, the 803 and 532 nm depletion indicated by the black pulse profiles in Fig. 7(a) and (b) was 66% and 45%, respectively, and the UV energy was $\sim$190 mJ. Installing a variable splitter to adjust the ratio of 532 nm energy used for amplification and for SFG resulted in 67% and 50% depletion, respectively, for 803 and 532 nm. Unfortunately, maximum UV energy fell to 180 mJ due to reflective and transmissive losses from additional optical elements. Lack of photon balance suggests incorrect SFG crystal length or 803 and 532 nm beams with poorly matched spatial modes or mismatched beam diameters, or some other unidentified efficiency-reducing mechanism. We tested SFG crystal lengths of 8 and 10 mm and found that the 8 mm crystal produced the greatest UV energy, so perhaps an even shorter crystal would produce more UV. Determining the degree of photon balance for intracavity SFG is complicated by the presence of two pump-depleting processes, and by a signal that circulates in the cavity, so we never attempted that measurement.

The UV-generating systems described here are complex, so questioning the need for pulsed self-seeded OPOs, Gaussian to flat-top beam shaping, and injection-seeded pump lasers, is reasonable. As the pulse profiles in Fig. 5(b) and (c) made clear, flat-topped beams are required for achieving pump depletion $\geq$65% in the OPO used in these tests. However, for high-efficiency SFG, we found near-zero OPO buildup time to be of equal or greater importance than achieving the highest possible OPO pump depletion. To demonstrate the importance of buildup time, the pulse profiles in Fig. 7(c) compare UV energy with and without pulse seeding, where it falls from 180 to 133 mJ, largely due to the reduction in temporal overlap of the 803 and 532 nm pulses.[2] An even further reduction in energy occurs

[2]In the experiment, there was no simple way to achieve forward-direction CW seeding, so with the pulsed-seed beam blocked, the OPO oscillates on multiple longitudinal modes. The OPO was pumped well above its unseeded threshold, so any reduction in signal energy was small, and the amplified multimode signal energy was comparable to the single-mode amplified signal energy. The mixing acceptance bandwidth for the 803 nm signal in 36.6° cut type II BBO is 8.15 cm·cm^{-1}, or about 10 cm^{-1} (300 GHz) for the 8-mm-long SFG crystal, which is at least 10× the multimode oscillation bandwidth of the KTP OPO. The important observation in this test was reduced UV energy resulting from increased OPO buildup time.

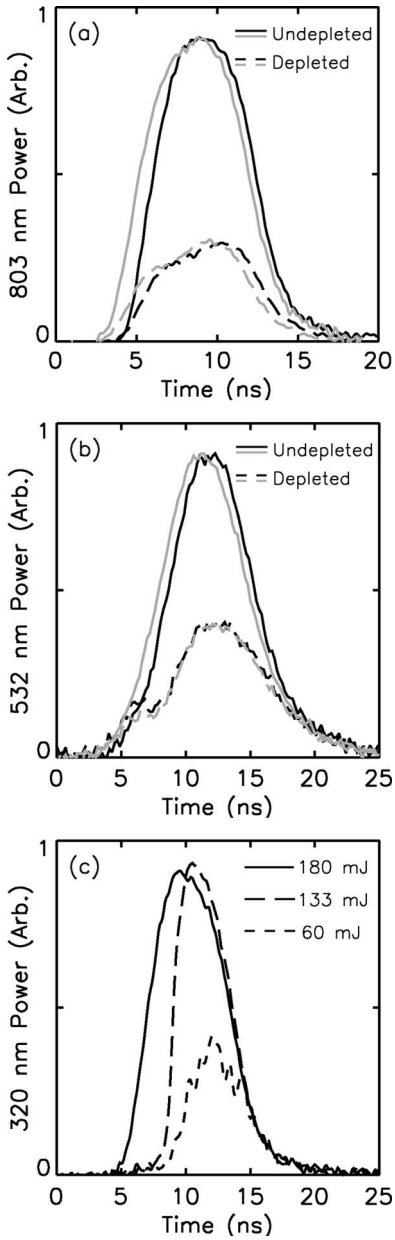

Fig. 7. The efficiency of SFG can be determined by comparing depletion of the pulses that are summed to generate UV light. (a) Depleted and undepleted 803 nm pulses. (b) Same for 532 nm. The black pulse profiles were recorded when the dashed 532-nm beamsplitter in Fig. 6 had $R = 50\%$, and the grey profiles—temporally offset for clarity—were recorded using a variable beam splitter. For the 50% splitter, 803 nm depletion was 66% and 532-nm depletion 45% with UV energy of ~190 mJ, and for the variable splitter, depletion was 67% and 50%, respectively, with UV energy of ~180 mJ. (c) High SFG efficiency requires self-seeding and injection-seeded pump lasers. Without self-seeding, UV energy drops from 180 to 133 mJ, and by using a multimode pump laser, it is further reduced to only 60 mJ. See text for additional details.

when the forward pump laser is allowed to oscillate on multiple longitudinal modes while the OPO remains unseeded. Mixing a deeply amplitude-modulated multimode pump pulse from the homogeneously broadened Nd:YAG laser with the pulse from an OPO pumped by this same laser reduces the UV energy to only 60 mJ.

As we have stressed all along, numerical modeling plays a central role in our designs, so asking if measured UV energy agreed with model predictions is also reasonable. For the extracavity system, we predicted 1064 to 320 nm efficiency approaching 25%, so there agreement is decent given the measured efficiency of about 21%. The model for the intracavity system predicts 532 to 320 nm efficiency exceeding 50%, or 1064 to 320 nm efficiency exceeding 35% using the measured 71% 2ω conversion efficiency, so agreement in this case is not as good. However, there are limits to the effectiveness of the models as they do not include absorptive heating and other higher order effects encountered in real devices. When all model input parameters are well known, and laboratory conditions limit influences such as absorptive heating, the models were shown to agree with the measurements at the 1%–3% level (see footnote 1) [7], [8]. However, large diameter beams, high Fresnel numbers, complex systems with many optical elements, and UV energies exceeding 100 mJ, all increase the importance of artifacts like absorptive heating, stray reflections, and scattering. For example, when the beam from the pulsed-seed optical network is interferometrically aligned to the OPO cavity, it sometimes generates a stray reflection that arrives ahead of, and out of phase with, the pulsed seed, thus reducing the OPO's signal beam quality. This effect was difficult to eliminate, but would never be included in a model, yet it affects conversion efficiency. A more serious problem was absorptive heating in BBO. With few exceptions, $\chi^{(2)}$ nonlinear optical crystals are poor heat conductors; however, some degree of temperature control is possible. Unfortunately, accurately modeling the effects of absorptive heating, including the effects of reducing heating with temperature control, is nearly impossible because temperature gradients in the crystal depend on boundary conditions that are rarely well known. Even though heating can strongly effect performance, it is usually better to measure its effects in the laboratory.

Although UV conversion efficiency was high for both configurations, we observed absorptive heating effects that we believe reduced efficiency and caused energy output to drift on approximately 10 s time scales. Some thermal effects were expected because it is well known that two-photon absorption occurs in BBO for $\lambda \lesssim 340$ nm [16], [17]. We made no attempt to directly measure increases in crystal temperature, but a combination of nonzero dn/dT and BBO's temperature-dependent phase velocity mismatch Δk are likely suspects for our observations. UV energies $\gtrsim$100 mJ for our ~6-mm diameter beams caused substantial changes in UV energy that were compensated for by adjusting crystal phase-matching angles. We found stable operation resumed by lowering pump energy or by angle tuning the SFG crystal to add enough Δk to reduce UV production. The band edge in BBO corresponds to approximately the energy of a single 170 nm photon, so with sufficiently high optical power two-photon absorption effects should be expected at $\lambda = 320$ nm. Numerous measurements of two-photon absorption in BBO appear in the literature, with examples being [16] and [17], but there appears to be no complete characterization of its β tensor.

Absorptive heating effects were especially strong for intracavity mixing, where the signal wave suffers substantial wavefront

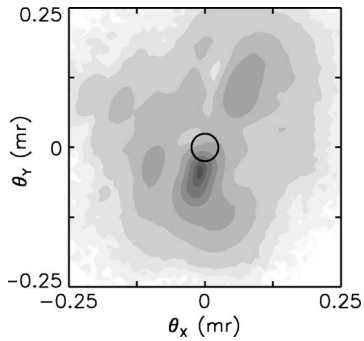

Fig. 8. Far-field 320 nm spatial fluence profile for intracavity SFG plotted against the far-field angles θ_x and θ_y. The black circle approximates the diffraction limit using $\lambda f/\# = \lambda fl/D \approx 52\,\mu$m with $fl = 1070$ mm and $D \approx 6.5$ mm, converted to far-field angle for this plot. Signal wavefront distortion from two-photon absorptive heating in the intra-cavity BBO crystal reduces beam quality and causes hot spots for UV energy of only 18 mJ. See text for additional details.

distortion by repeatedly passing through the heated BBO SFG crystal. Fig. 8 illustrates these effects, where the 320 nm far-field fluence for intracavity SFG is segmented into hot spots for UV energy of only 18 mJ. At higher UV energies, the distortion worsens and beam quality suffers accordingly. In the absence of signal-wave distortion, the 320 nm fluence in Fig. 8 might resemble the 803 nm far-field fluence in Fig. 1(b). We note that for extracavity SFG the signal wave passes through the crystal only once so distortion effects are present, but not as strong as in Fig. 8. Absorptive heating for $\lambda \geq 300$ nm may be reduced by replacing BBO with lithium triborate (LBO). The single-photon band edge in LBO should be closer to 160 nm and the measured two-photon absorption in LBO at 264 nm is reported to be five to six times smaller than in BBO [18].

VI. Current and Future Work

The extra- and intracavity SFG configurations described in Section IV performed well but both require modification to facilitate the transition from laboratory to deployable systems. To this end, modifications we are currently testing include replacing the KTP crystals in the OPO's with BBO to achieve higher radiation hardness, using unequal length OPO crystals to obtain better control over the onset of back-conversion, testing pulsed idler seeding using an auxiliary source in place of backward-pumped self-seeding at the signal wavelength, using a single pump laser for the entire system, obtaining higher 2ω conversion efficiency, replacing the bulky Ti:sapphire CW seed laser with a compact grating-tuned diode laser, and replacing the extracavity BBO crystal with LBO. Future modifications might include replacing the BBO SFG crystal in the intracavity system with LBO to reduce two-photon absorption effects and replacing vibration-sensitive grating tuned diode lasers with fiber-coupled distributed feedback (DFB) lasers. We are currently evaluating the advantages and disadvantages of some of these modifications.

Given the possibility of satellite deployment, the radiation environment of low-Earth orbit may limit or prohibit the use of the crystal KTP. However, BBO and its isomorphs such as LBO exhibit higher radiation hardness than does KTP [19]. We replaced type II KTP with type II BBO, but it requires modifying the OPO because $d_{\text{eff}} = 1.62$ pm/V for the 27.4° cut of BBO compared to $d_{\text{eff}} = 3.22$ pm/V for 58.4° xz-cut KTP. In addition, BBO's e- and o-wave polarizations are rotated by 90° with $532(\text{e}) \rightarrow 1576.4(\text{e}) + 803(\text{o})$. A $1.5\times$ larger RISTRA OPO assembly holds longer crystals required to compensate for BBO's smaller d_{eff}, and a different cavity mirror set, along with the reversed direction of propagation in the cavity, accommodates the 90° rotated eigenpolarizations. We also selected a shorter first crystal, followed by a longer second crystal, to maximize gain while achieving lower back-conversion. Modeling suggests BBO crystal lengths of 13 and 20 mm to produce a signal energy of 120–150 mJ with little back-conversion.

We showed that backward-pumped self-injection seeding at the signal wavelength is effective for achieving high pump depletion and near zero cavity buildup time in ns OPOs. However, it requires extra-optical elements, including three expensive large-bore isolators—one for the seed optical network and two for the pump beams—and it also involves the complex geometry of coupling the backward propagating pump beam into the nonplanar RISTRA cavity. In addition, amplified stray signal reflections in the seed-beam optical network might diminish beam quality. As an alternative to self-seeding, we are testing pulsed idler seeding using a RISTRA OPO as the auxiliary source, where the nonresonant idler seeds the high-energy OPO to generate a resonant signal wave. However, using an auxiliary OPO as a seed source requires two stages of frequency stabilization: the auxiliary OPO must be locked to a CW seed laser and the CW seed laser's frequency must be controlled to maximize the high-energy OPO's output. Step-wise dithering of the CW seed frequency at the pump laser's repetition rate generates the error signal for maximizing the high-energy OPO's signal output, while the auxiliary OPO follows the frequency of its CW seed using Pound–Drever–Hall stabilization [20], [21]. Two advantages of pulsed idler seeding are fewer stray reflections and the use of compact telecommunications DFB lasers as CW seed sources. However, disadvantages include additional frequency stabilization electronics, and an initial alignment procedure that is more difficult than that required for self-seeding. For idler seeding, the frequency of the pulsed-idler beam must be tuned to generate a resonant signal wave in the high-energy OPO, and it must also be interferometrically aligned to this cavity. Absence of these two signatures before the onset of oscillation in the high-energy OPO makes initial alignment difficult. Until we complete current development work, we cannot definitively say whether idler seeding or signal self-seeding is the preferred method.

Using a single pump laser rather than two removes the convenience of electronic control of the relative pulse arrival times, but is otherwise a straightforward modification that simplifies the system. We also now obtain higher 2ω efficiency from our pump laser by replacing our 10-mm-long type II KTP crystals with 20-mm-long crystals. At the same time, we also increased the pump beam diameter from 6–7 mm to 8–8.5 mm. With the high-quality flat-topped 1064 nm beam, we obtain at least 82% 2ω efficiency. Finally, we replaced the extracavity BBO SFG

crystal with LBO to reduce absorptive heating effects. The only disadvantage of LBO is its small d_{eff}, 0.58 pm/V compared to 1.95 pm/V for type I BBO, requires a large and expensive crystal.

For our current efforts, we've abandoned intracavity SFG because of two-photon absorptive heating in BBO. However, in the future, the intra-cavity BBO crystal might be replaced with LBO, which may reduce or eliminate UV absorption. Unfortunately, LBO phase matches for type I mixing only, and type II mixing in the OPO crystal must be retained for optimum beam quality. Consequently, using LBO requires intracavity retarders capable of switching signal and pump polarizations between type I and type II mixing. This can be achieved using a two-plate optically contacted retarder with the first plate having retardation of λ_{pump}, $\lambda/2_{\text{signal}}$ or perhaps λ_{signal}, $\lambda/2_{\text{pump}}$, and the second having retardation of $\lambda/2$ for both waves, with the plate axes oriented relative to each other at 22.5°, as required by the RISTRA cavity's geometry. The crystal bismuth triborate (BiBO) may also offer a solution as it phase matches for type II mixing. However, BiBO's two-photon absorptive properties may not be well known, so its suitability is speculative. Using either LBO or BiBO may be worth investigating as intracavity SFG requires fewer optical elements, less optical alignment, and has higher efficiency than that of extracavity SFG.

Finally, we mentioned DFB lasers as CW seed sources when discussing idler seeding. DFB lasers are attractive because they are compact, vibration-resistent, fiber-coupled, can be directly phase modulated, are available for wide range of telecommunication wavelengths, and consume little power. For generating 320 nm light, there are two ways to employ these lasers. Pulsed idler seeding using a 1064-nm pumped auxiliary OPO requires a CW seed wavelength of 1576 nm, which may be available. Self-seeding at the signal wavelength requires 803 nm, which is probably not available, but could be obtained by frequency doubling a 1606 nm laser in a stabilized buildup cavity. To generate 308 nm light requires either 1950.7 nm for pulse idler seeding, which is probably not available, or 731.5 nm for self-seeding at the signal wavelength, which could be obtained by frequency doubling a 1463 nm laser, which is available.

VII. Conclusion

We generated $\sim$10 ns duration pulses at $\lambda = 320$ nm with energies in the range of 160–200 mJ and optical-to-optical efficiencies $>20\%$ using two different Nd:YAG-pumped OPO-based laboratory prototype UV-generation systems. The key technical features of our systems are the use of image-rotating nonplanar ring-cavity OPOs to produce high-quality output beams, pulse injection seeding of the OPOs to reduce cavity buildup time to near zero for enhanced SFG efficiency, and the use of high-quality flat-topped beam profiles for pumping the OPOs and for injection-seeding the OPOs. Two experimental configurations were tested: one referred to as "extracavity," where SFG occurs in a crystal separate from the OPO cavity and the other referred to as "intra-cavity," with the SFG crystal inside the OPO cavity to take advantage of the cavity-enhanced signal fluence. For both configurations, the OPOs were pumped by the 532 nm second harmonic of Nd:YAG to generate a tunable 803 nm signal wavelength that is subsequently mixed with additional 532 nm light to generate UV at 320 nm. Maximum UV energies and efficiencies were $>$190 mJ and 21%, and 160 mJ and 24%, respectively, for extracavity and intracavity configurations.

Our system designs result from an integrated approach where all operating parameters including the pump-beam spatial profile, the second harmonic generation efficiency, the OPO's cavity geometry, output coupling, and crystal lengths, and the length of the SFG crystal, are all obtained from numerical modeling. By further optimizing operating parameters, we expect to eventually generate UV pulse energies approaching 300 mJ with optical conversion efficiencies comparable to those already achieved.

The intended application for these UV generators is deployment in airborne or satellite-based UV ozone DIAL remote-sensing systems. Although our current laboratory prototypes generate only 320 nm light, a second wavelength closer to 300 nm required for ozone DIAL can be obtained by changing crystals, OPO cavity optics, and other associated optical elements.

Acknowledgment

The authors would like to thank R. Allman, Principal Technologist in Department 1128, Sandia National Laboratories, for technical assistance in the laboratory.

References

[1] A. Fix and G. Ehret, "Intracavity frequency mixing in pulsed optical parametric oscillators for the efficient generation of continuously tunable ultraviolet radiation," *Appl. Phys. B*, vol. 67, pp. 331–338, 1998.

[2] A. V. Smith and M. S. Bowers, "Image-rotating cavity designs for improved beam quality in nanosecond optical parametric oscillators," *J. Opt. Soc. Amer. B*, vol. 18, pp. 706–713, 2001.

[3] D. J. Armstrong and A. V. Smith, "Demonstration of improved beam quality in an image-rotating optical parametric oscillator," *Opt. Lett.*, vol. 27, pp. 40–42, 2002.

[4] A. V. Smith and D. J. Armstrong, "Nanosecond optical parametric oscillator with 90° image rotation: Design and performance," *J. Opt. Soc. Amer. B*, vol. 19, pp. 1801–1814, 2002.

[5] D. J. Armstrong and A. V. Smith, "90% pump depletion and good beam quality in a pulse-injection-seeded nanosecond optical parametric oscillator," *Opt. Lett.*, vol. 31, pp. 380–382, 2006.

[6] D. J. Armstrong and A. V. Smith, "Using a Newport refractive beam shaper to generate high-quality flat-top spatial profiles from a flashlamp-pumped commercial Nd:YAG laser," *Proc. SPIE*, vol. 5525, pp. 88–97, 2004.

[7] A. V. Smith and M. S. Bowers, "Phase distortions in sum- and difference-frequency mixing in crystals," *J. Opt. Soc. Amer. B*, vol. 12, pp. 49–57, 1995.

[8] A. V. Smith, W. J. Alford, T. D. Raymond, and M. S. Bowers, "Comparison of a numerical model with measured performance of a seeded, nanosecond KTP optical parametric oscillator," *J. Opt. Soc. Amer. B*, vol. 12, pp. 2253–2267, 1995.

[9] G. Anstett, M. Nittman, and R. Wallenstein, "Experimental investigation and numerical simulation of the spatio-temporal dynamics of the light-pulses in nanosecond optical parametric oscillators," *Appl. Phys. B*, vol. 79, pp. 305–313, 2004.

[10] A. J. Campillo, "Internal upconversion and doubling of an optical paramtric oscillator to extend the tuning range," *IEEE J. Quantum Electron.*, vol. QE-8, no. 12, pp. 914–916, Dec. 1972.

[11] G. T. Moore and K. Koch, "Optical parametric oscillations with intracavity sum-frequency generation," *IEEE J. Quantum Electron.*, vol. 29, no. 3, pp. 961–969, Mar. 1993.

[12] E. C. Cheung, K. Koch, and G. T. Moore, "Frequency upconversion by phase-matched sum-frequency generation in an optical parametric oscillator," *Opt. Lett.*, vol. 19, pp. 1967–1969, 1994.

[13] A. Shirakawa, H. W. Mao, and T. Kobayashi, "Highly efficient generation of blue-orange femtosecond pulses from intracavity-frequency-mixed optical parametric oscillator," *Opt. Commun.*, vol. 123, pp. 121–128, 1996.
[14] G. T. Moore and K. Koch, "Optical parametric oscillation with detuned intra-cavity sum-frequency generation," *IEEE J. Quantum Electron.*, vol. 29, no. 8, pp. 2334–2341, Aug. 1993.
[15] Y. Dikmelik, G. Akgün, and O. Aytür, "Plane-wave dynamics of optical parametric oscillation with simultaneous sum-frequency generation," *IEEE J. Quantum Electron.*, vol. 35, no. 6, pp. 897–912, Jun. 1999.
[16] R. DeSalvo, A. A. Said, D. J. Hagan, E. W. VanStryland, and M. Sheik-Bahae, "Infrared to ultraviolet measurements of two-photon absorption and n_2 in wide bandgap solids," *IEEE J. Quantum Electron.*, vol. 32, no. 8, pp. 1324–1333, Aug. 1996.
[17] L. I. Isaenko, A. Dragomir, J. G. McInerney, and D. N. Nikogosyan, "Anisotropy of two-photon absorption in BBO at 264 nm," *Opt. Commun.*, vol. 198, pp. 433–438, 2001.
[18] A. Dubietis, G. Tarnošauskas, A. Varanavičius, and G. Valiulis, "Two-photon absorbing properties of ultraviolet phase-matchable crystals at 264 and 211 nm," *Appl. Opt.*, vol. 39, pp. 2437–2440, 2000.
[19] U. Roth, M. Tröbs, T. Graf, J. E. Balmer, and H. P. Weber, "Proton and gamma radiation tests on nonlinear crystals," *Appl. Opt.*, vol. 41, pp. 464–469, 2002.
[20] R. W. P. Drever, J. L. Hall, F. V. Kowalski, J. Hough, G. M. Ford, A. J. Munley, and H. Ward, "Laser phase and frequency stabilization using an optical resonator," *Appl. Phys. B*, vol. 31, pp. 97–105, 1983.
[21] E. D. Black, "An introduction to Pound–Drever–Hall laser frequency stabilization," *Amer. J. Phys.*, vol. 69, pp. 79–87, 2001.

Darrell J. Armstrong received the B.S. degree in physics from the University of Washington, Seattle, in 1987, and the Ph.D. degree in physics from the University of Colorado, Boulder, in 1993.

Since 2001, he has been with Sandia National Laboratories, Albuquerque, NM, where he was a Postdoctoral Fellow from 1993 to 1996. His current research interests include applications of nonlinear optics for developing remote-sensing light sources. He is a codeveloper of the rotated image singly-resonant twisted rectangle (RISTRA) optical parametric oscillator (OPO).

Arlee V. Smith received the B.S. degree in physics from Alma College, Alma, MI, in 1969, and the Ph.D. degree in physics from the University of Michigan, Ann Arbor, in 1977.

He was a Postdoctoral Fellow at JILA. He joined Sandia National Laboratories, Albuquerque, NM, in 1980. His current research interests include nonlinear optics and numerical modeling of fiber lasers. He is the author of the SNLO nonlinear optics software package.

Dr. Smith is a Fellow of the Optical Society of America.